Characterization of Inkjet-printed Explosive Materials on various surfaces

Mikella E. Farrell, Ellen L. Holthoff, Logan S. Marcus, and Paul M. Pellegrino
U.S. Army Research Labs, RDRL-SEE-E, 2800 Powder Mill Rd., Adelphi, MD 21228

ABSTRACT

The requirement to detect hazardous materials at both point and standoff distances has led to the development of laser-based hazard detection systems with immediate application for the security and safety of the US military, national security agencies, and environmental response teams. In particular, common explosive and improvised explosive device (IED) materials have motivated research efforts toward detecting trace (<100 µg/cm^2) and bulk (>100 µg/cm^2) quantities of these threats on multiple surfaces. Test coupons must demonstrate realistic concentrations, mimic real life particle sizes, and be fabricated on a host of substrate materials in order to evaluate the ability of these systems to accurately detect and identify hazard materials.

Keywords: explosive, Raman, ink jet printing, ammonium nitrate, hazard

1 INTRODUCTION

The requirement to detect hazardous materials has led to the development of hazard detection systems with immediate application to the US military, national security agencies, and environmental response teams. In particular, it has been demonstrated that the detection of common explosives and improvised explosive devices (IED) substance particles on a host of materials including natural and manmade textiles, metals, and plastics; and naturally occurring materials like wood, stone, hair, or even skin can be an indicator of either suspicious objects or subjects. There are some standard techniques used for the detection of quantities of explosive materials, however many of them are both labor, skill expensive and require significant time for sample analysis. An alternative technique that does not require sample preparation or destruction is Raman

One of many spectroscopic techniques gaining increased attention for the detection of hazard materials, Raman has generated significant interest[1-3]. The unique chemical "fingerprint" provided by Raman techniques allow for chemical identification within a complex environment. Additionally this is a technique that can apply to both standoff detection and bench top forensic hazard investigations. Raman spectroscopy[4-10] is a detection technique generally used to measure the vibrational, rotational and low frequency modes in a system. Generally the interrogation light used is a monochromatic source like a laser. The laser light interacts with the molecule resulting in a frequency shift (increase or decrease) relative to the energy of the vibrating molecules. Advantages of using Raman-based detection techniques are that little to no sample preparation is necessary, there is little to no sample degradation, only a small quantity of material is needed, several different laser sources can be used, the technique is fairly insensitive to environmental conditions (like water interference), and it can generate a "fingerprint" spectrum from which sample identification and quantification is possible. With all of these advantages, Raman has been shown to be a reliable means of Army and first responder relevant hazard detection with paramount features including preservation of samples for additional forensic testing.[6, 11]

There are many examples of hazardous materials encountered by the US military and first responders. Some examples of common explosives include octogen (HMX), 1,3,5-trinitroperhydro-1,3,5-triazine (RDX), 2,4,6-trinitrotoluene (TNT), and black powder. Common examples of IED/ homemade explosive (HME) components can include ammonium nitrate and urea. Many of these materials have well known Raman signatures that can be used for stand-off detection and identification. Some of these materials are also known to exist in multiple polymorphic phases[7, 12-25] that can in part be attributed to concentration levels of material present, handling and storage methods used, and in some certain cases even the surface onto which the material has been deposited. Generally in fingerprints, explosive material particle sizes range from 10 µm to several hundred µms; with the bulk of the sample consisting of smaller sized particles. To validate the ability to measure these small particles, it is necessary to use a standardized deposition technique (like inkjet printing) that can deliver known particle masses and particle sizes.

Inkjet printing[8, 19, 26, 27] is increasingly being used as a standardized means to create samples for the training and evaluation of hazard detection systems. Using an inkjet printer system, the user is able to deposit material (ranging from trace (<100 µg/cm^2) to bulk (> 100 µg/cm^2) in specific locations, and deposit known volumes to each of those locations. Inkjet printing technologies have in part replaced some other means of coupon sample fabrication like drop and dry methods because they are more reliable, accurate and reproducible. Inkjet printed samples can be

fabricated on several different substrate surfaces including natural and manmade materials.

For this paper we demonstrate that inkjet technologies can be used to deposit material on a host of substrate types, and Raman spectroscopy can be used for the successful detection and identification of the IED material ammonium nitrate on these substrates. The material ammonium nitrate was selected because it is a common fertilizer component that is useful in agricultural and industrial applications, and the production of HMEs and IEDs. Ammonium nitrate in pure format is generally described as a white crystalline material at standard temperature and humidity. Ammonium nitrate (AN) has been previously shown to exist in at least five different crystal phases.[7] In this paper, Raman spectral information of AN at both a bulk (>100 µg/cm^2) and trace (<100 µg/cm^2) concentrations is inkjet deposited into differing substrates including silicon, aluminum, polyethylene, various cloth materials, and human hair substrates is reported.

2 EXPERIMENTAL

2.1 Reagents and Materials.

AN, methanol (MeOH), ethanol (EtOH), and distilled water were obtained from Sigma-Aldrich. All AN inkjet solutions were prepared at various concentrations in solvents of water, methanol or a mixture of these solvents. All solvents used were HPLC grade. All chemicals were used as received unless otherwise noted.

2.2 Printed Material Substrates.

Velveteen squares were procured from ScienceWare (catalog # 37848-001, off white tan) and were used as received. Poljean Cleaning Cloth samples were procured from TedPella (catalog 381224, white matte finish) and used as received. Hair samples were procured from Hair imports (Gendale, NY). The hair material (Uzbecki brown hair) was used as received. The tarp sample was VWR and is described as top tarp white. Squares of material were cut from the larger sample. Samples were used as received. The polyethylene (PE) sample was cute from a larger sheet material. The silicon (Si) sample was cut from a larger Si wafer in house. Used as received without additional cleaning. Aluminium samples were purchased from www.onlinesheetmetal.com. Samples were cut to small 1 inch squares, and were gently wiped clean with ethanol prior to use.

2.3 Instrumentation

Scanning electron microscope (SEM) images was obtained using a FEI environmental SEM (Quanta 200 FEG).

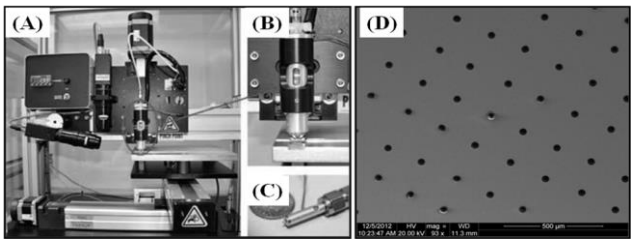

Figure. 2. Photographs of (A) JetLab 4 drop-on-demand inkjet printing platform (B) dispensing device and ink solution encasement; and (C) print head assembly. In (D) SEM image of a printed AN sample demonstrating clear, distinct, uniform rows of printed materials.

Printed materials were produced using a JetLab® 4 (MicroFab Technologies) tabletop printing platform and have been previously documented.[28] Briefly, the JetLab® 4 is a drop-on-demand inkjet printing system with drop ejection drive electronics (JetDrive™ III), pressure control, a drop visualization system, and precision *X*, *Y*, *Z* motion control. The dispensing device (print head assembly, MJ-AL-01-060) consists of a glass capillary tube, with a 60 µm diameter orifice coupled to a piezoelectric element. Voltage pulses (20–25 V; rise time 1 µs; dwell time 28–32 µs; fall time 1 µs) applied to the piezo result in pressure fluctuations around the capillary. These pressure oscillations propagate through the printing fluid in the tube, resulting in ejection of a microdrop. Drops are visualized using synchronized strobe illumination and a charged coupled device (CCD) camera. Determining optimal jetting parameters is a trial-and-error process. Stable droplet ejection is achieved by visually observing expelled microdrops and adjusting voltage pulse parameters and capillary fluid backfill pressure. Conditions that provide the highest drop velocity without satellite droplet formation are desired. Printing was performed at a frequency of 250 Hz with a droplet velocity of ~2 m/s. Drop diameter was estimated to be ~60 µm, based on the capillary orifice diameter. During printing, a single substrate was placed on the sample stage. The print head remained fixed at a specified height while the stage moved to print a specified pattern. A rectangular array, which covers a rectangular area with rows of equidistant points, was pre-programmed based on the substrate size and desired sample concentration. An array pattern was chosen for the purpose of creating the effect of a homogeneous coating for optical interrogation. Depending on the desired concentration per unit area (e.g., µg/cm^2), the total number of drops needed to achieve the desired concentration in that area was calculated based on the mass of a single microdrop. Based on the number of total drops needed, the array spacing and drops needed per line can be calculated. These values are easily adjusted depending on concentration. Arrays were printed using the print on-the-fly mode. In this mode, the stage moves continuously as a single microdrop is dispensed at each array element. Print on-the-fly mode improves sample throughput. Concentrations of deposited

materials have been validated using a secondary UV-Vis measurement. This method has been previously documented, and typically has R^2 values above 0.998 and RSDs of <3% or better. [27, 28]

2.4 Raman Measurements.

Raman data was recorded using a Renishaw inVia Reflex Raman microscope equipped with a near-infrared diode laser excitation source (λ = 785 nm). The light from the diode was focused onto the samples at the microscope stage through a 5X objective. A 5X or 20X objective was used for all measurements unless otherwise noted. Dispersion and resolution of the Renishaw vary with wavelength, but are typically 1 cm^{-1}, decreasing to 0.5 cm^{-1} for certain gratings and wavelengths. Prior to coupling into the microscope, the diode laser beam was circularized by inserting a pinhole into the optical beam path and neutral density filters were used resulting in reduction of the maximum available laser power to 7 mW. Samples at the microscope stage were positioned remotely with a joystick using an encoded, motorized *XYZ* translation stage (0.1 µm step size) controlled by a Prior Scientific ProScan II controller. WiRE 3.2 software, operating on a bench top computer, was used for instrument control and data collection. Before all measurements, the instrument was wavelength calibrated using an internal silicon standard. Data analysis was completed using IgorPro 6.0 software (Wavemetrics).[29]

3 RESULTS AND DISCUSSION

The Army and first responders have a keen interest in identifying potential hazards on a host of commonly encountered items/substrates. With this in mind, we were interested to determine if when using the inkjet system, it would be possible to fabricate AN materials on various surfaces and detect the printed materials. To test this hypothesis the experiments discussed in the following sections were conducted.

To characterize how AN samples set up on various materials, we inkjet printed several concentrations of AN onto silicon, aluminum, polyethylene, various cloth materials, and human hair substrates. These materials all have different wicking capabilities, rigidness, and are therefore assumed to interact differently with the AN solution printed. The printed materials were physically characterized with SEM measurements, and were also spectrally characterized by Raman measurements. The results for these various experiments will be discussed in the following sections.

In these experiments a high and low concentration of AN was inkjet printed onto the following surfaces: silicon, aluminum, polyethylene, cloth materials, velveteen, tarp, and human hair. These materials were selected as they represent both natural and manmade materials. For these inkjetted materials, a standard wave form was used with a Dwell time set at 34 us, echo time at 32 us, Dwell voltage at 21, Echo voltage at -19, and a pressure set point set at -0.07 psi. Using these settings it was possible to consistently produce a uniform "good" droplet. To print the materials at the two desired concentrations, the parameters in Table 2 were followed. For these experiments both the spacing, and number of drops in the X direction were varied to produce a final sample concentration of 10 µg/cm^2 (representing trace) and 1000 µg/cm^2 (representing bulk). For these experiments, and AN solution concentration of 1.20 M was simultaneously inkjet printed onto the substrate surfaces under investigation.

To characterize how the printed material "looked" on the substrate surface a series of digital camera and SEM images were collected. See Figure 3 for an example photo image and SEM image of substrate materials onto which AN was printed. In Figure 3, photo and SEM images of (A,B) velveteen, (C, D) cloth, (E, F) hair, (G, H) Tarp, (I,J) aluminum, (K, L) silicon, and (M,N) PE are shown. These materials have AN printed on them at concentrations of either 10 ug/cm^2 or 1000 ug/cm^2. In SEM figure B, D, F, and H it is challenging to see the printed AN material on the substrate surface. This may due to some of these materials being more "absorbent" of wet materials (B, D, F) as compared to some of the more rigid surfaces (J, L, N). Also due to the surface interactions between the substrate and the AN, physically different depositions of AN appear to have formed on some of the more rigid surfaces. For comparison, consider J, L and N (all printed under same conditions at same time). In these SEM images, the AN printed materials appear as either "crunchy" rows, a random dispersion of large and small features, or a somewhat uniform (size and spacing) array of material.

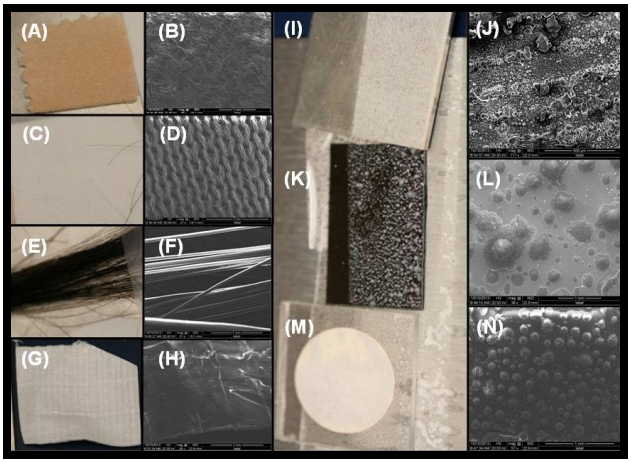

Figure. 3. Photo and SEM images of (A,B) velveteen, (C, D) cloth, (E, F) hair, (G, H) Tarp, (I,J) aluminum, (K, L) silicon, and (M, N) PE. These materials have AN printed on them at concentrations of either 10 ug/cm^2 or 1000 ug/cm^2. Due to the surface interactions between the substrate and the AN, physically different depositions of

AN appear to have formed, compare J, K and M (all printed under same conditions at same time).

To physically characterize the nature of the actual AN droplet on rigid surface, SEM images were collected of individual AN deposits. In Figure 4A, a representative AN droplet from a 10 µg/cm^2 printed solution concentration is shown. This droplet is approximately 50 µm in diameter, and appears to have an outer crystalline structure surface. This image is an example of how the uniform droplets generally appear when printed on a rigid surface with adequate spacing and drying times.

For all Raman measurements, it was necessary to first determine a spectral baseline of the substrate material, and then collect data from the two deposited AN concentrations. In Figure 4B-D, the Raman data for a baseline substrate (Si, Al and PE), 10 µg/cm^2 AN, and 1000 µg/cm^2 AN concentration are all shown. In Figure 4B, Raman silicon has a broad band located between 922 cm^{-1} and 1000 cm^{-1}. The signal of the 1000 µg/cm^2 AN as compared to the 10 µg/cm^2 AN is approximately 9X larger. The starred peak reflects the AN band symmetric stretch mode of NO_3^- located at 1043.2 cm^{-1} for the 10 µg/cm^2 Raman band, and 1044.2 cm^{-1} for the 1000 µg/cm^2 Raman band. In Figure 4C, the background and Raman data for AN on aluminum is shown. In this figure, the starred band is located at 1042.3 cm^{-1} for the 10 µg/cm^2 Raman band, and 1044.2 cm^{-1} for the 1000 µg/cm^2 Raman band. Polyethylene has main bands occurring at 630.47 cm^{-1}, 702.99 cm^{-1}, 857.08 cm^{-1}, 1117.1 cm^{-1}, 1175.0 cm^{-1}, 1283.60 (C-H twisting) cm^{-1}, 1614.1 cm^{-1}, and 1724.60 cm^{-1}. In this figure, the starred band is located at 1042.3 cm^{-1} for the Raman band, and 1042.3 cm^{-1} for the Raman band. Considering the resolution of the instrument, these bands are both exhibiting the same phase IV of AN. It is hypothesized that some of the AN band shifting ranging from 1042 to 1044 cm^{-1} is attributable to some moisture in the samples.

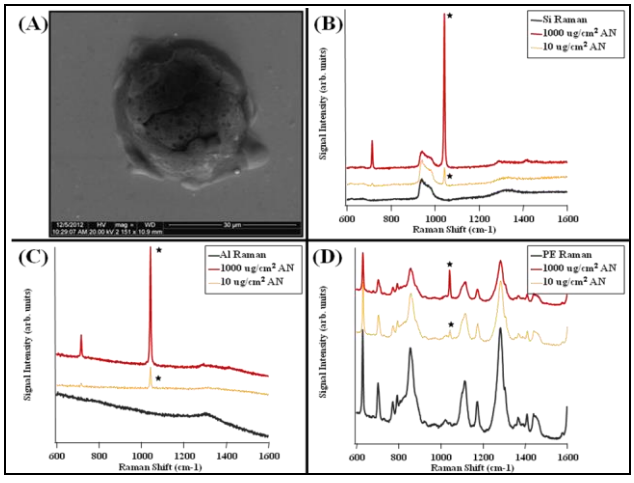

Figure. 4. In (A) a SEM image of a printed AN sample is shown, the Raman response to (B) Silicon, (C) Aluminum, and (D) polyethylene plastic is shown. In (B to D), the spectral Raman signatures from the blank material, 1000 µg/cm^2, and 10 µg/cm^2 AN printed samples are shown. The main AN band is designated with a star.

In Figure 5A-D, the Raman data for a baseline, 10 µg/cm^2 AN, and 1000 µg/cm^2 AN concentration are all shown for cloth, velveteen, plastic tarp material and finally human hair. In Figure 5A, the spectral data for cloth is shown. Cloth has main Raman bands located at 631.49 cm^{-1}, 702.99 cm^{-1}, 859.05 cm^{-1}, 999.24 cm^{-1}, 1095.4 cm^{-1}, 1291.8 cm^{-1}, 1418.4 cm^{-1}, 1615.8 cm^{-1}, and 1727.9 cm^{-1}. In this figure, the starred band is located at 1043.3 cm^{-1} for the 1000 µg/cm^2 AN sample. In figure 5B, the spectral data for Velveteen is shown. Velveteen has background Raman bands located at 1096.4 cm^{-1}and 1121.8 cm^{-1}. Velveteen with 1000 µg/cm^2 AN has a main band located at 1043.3 cm^{-1}. No AN was detectable at the lower concentration. It is possible that because of the absorbent nature of these materials, the AN solution is being wicked into the material. Therefore the lower concentration AN deposits are much more challenging to detect as compared to the higher bulk concentration.

In Figure 5C, Raman data for plastic tarp material is shown. Tarp has spectral bands located at 608.83 cm^{-1}, 1062.3 cm^{-1}, 1086.0 cm^{-1}, 1128.4 cm^{-1}, 1295.4 cm^{-1}, 1416.6 cm^{-1}, and 1439.6 cm^{-1}. In this figure, the starred band is located at 1042.3 cm^{-1} for the 10 µg/cm^2 AN sample, and 1044.2 cm^{-1} for the 1000 µg/cm^2 AN sample. In Figure 4D, the Raman spectral data from human hair is shown. In this figure, there is significant fluorescence background from the material. Due to the large background fluorescence, only the higher concentration 1000 µg/cm^2 AN sample has a measurable Raman band located at 1044.20 cm^{-1} (under the test conditions outlined in this proceedings paper).

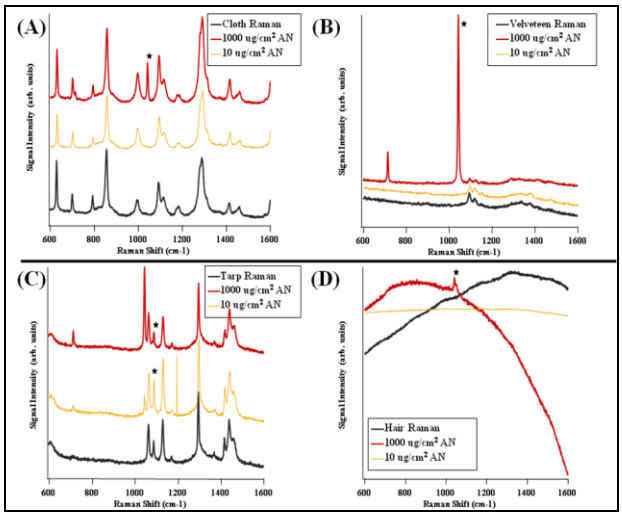

Figure 5. The Raman response to (A) cloth, (B) Veleveteen, (C) tarp, and (D) human hair is shown. The spectral Raman signatures from the blank material, 1000 µg/cm^2, and 10 µg/cm^2 AN printed samples are shown. The main AN band is designated with a star.

Table 1. Summary Raman signatures collected from several substrates inkjetted with AN at different concentrations.

Substrate Type	Background Material Raman Bands	AN Raman 10 µg/cm^2	AN Raman 100 µg/cm^2
Silicon	Broad band located between 922 cm^{-1} and 1000 cm^{-1}	1043.2 cm^{-1} Phase IV AN	1044.2 cm^{-1} Phase IV AN
Aluminum	1303.6 cm^{-1}	1042.3 cm^{-1} Phase IV AN	1044.2 cm^{-1} Phase IV AN
Polyethylene	630.47 cm^{-1}, 702.99 cm^{-1}, 857.08 cm^{-1}, 1117.1 cm^{-1}, 1175.0 cm^{-1}, 1283.60 (C-H twisting) cm^{-1}, 1614.1 cm^{-1}, and 1724.60 cm^{-1}	1042.3 cm^{-1} Phase IV AN	1042.3 cm^{-1} Phase IV AN
Cloth	631.49 cm^{-1}, 702.99 cm^{-1}, 859.05 cm^{-1}, 999.24 cm^{-1}, 1095.4 cm^{-1}, 1291.8 cm^{-1}, 1418.4 cm^{-1}, 1615.8 cm^{-1}, and 1727.9 cm^{-1}.	Not detectable	1043.3 cm^{-1} Phase IV AN
Velveteen	1096.4 cm^{-1}and 1121.8 cm^{-1}	Not detectable	1043.3 cm^{-1} Phase IV AN
Tarp	608.83 cm^{-1}, 1062.3 cm^{-1}, 1086.0 cm^{-1}, 1128.4 cm^{-1}, 1295.4 cm^{-1}, 1416.6 cm^{-1}, and 1439.6 cm^{-1}	1042.3 cm^{-1} Phase IV AN	1044.2 cm^{-1} Phase IV AN
Human Hair	Broad Fluorescence band	Not detectable	1044.20 cm^{-1} Phase IV AN

4 CONCLUSIONS

In this paper efforts to characterize the nature of AN signatures observed on several different types of substrate were conducted. AN was inkjet printed onto several common materials (silicon, aluminum, polyethylene, various cloth materials, and human hair) at both a bulk (>100 µg/cm^2) and trace (<100 µg/cm^2) concentrations. We were able to demonstrate that trace AN could be measured on several of the surfaces, and characterize the AN phase present (generally phase IV was observed). Please remember that from these measurements, no attempt was made to characterize the starting analyte material, or comment on how the sample handling methods may impact the final product measured.

As described in the results section, we were able to measure trace AN inkjet deposited onto the following materials silicon, aluminum, polyethylene, and various cloth materials. Bulk AN material was able to be measured on the following substrate surfaces: silicon, aluminum, polyethylene, various cloth materials, and human hair.

Accurately training standoff detection systems for energetic hazards materials remains a priority. While AN is still extensively used, due to the increased restrictions on the import of it into theatre, a new threat is emerging, potassium chlorate. According to the a more recent article in USA today,[30] "*Potassium chlorate has surpassed fertilizer as the explosive of choice for insurgents, Pentagon research shows. For the first time in the 12-year war, potassium chlorate was the most common ingredient, fueling 60% of the IEDs."* Just as with AN, it is necessary to understand how working with this material and inkjet depositing it onto surfaces may impact the specific Raman signatures that are measured. Future works will include characterizing other common IED precursors to better understand how they interact with their environment.

REFERENCES

[1] J. C. Carter, S. M. Angel, M. Lawrence-Snyder, J. Scaffidi, R. E. Whipple, J. G. Reynolds, "Standoff detection of high explosive materials at 50 meters in ambient light conditions using a small Raman instrument," Applied Spectroscopy 59, 769 (2005).

[2] D. S. Moore, "Instrumentation for trace detection of high explosives," Review of Scientific Instruments 75, 2499 (2004).

[3] J. I. Steinfeld, J. Wormhoudt, "Explosives detection: A challenge for physical chemistry," Annual Review of Physical Chemistry 49, 203 (1998).

[4] J. J. Brady, M. E. Farrell, P. M. Pellegrino, "Discrimination of chemical warfare simulants via multiplex coherent anti-Stokes Raman scattering and multivariate statistical analysis," Optical Engineering 53, (2014).

[5] M. Farrell, E. Holthoff, P. Pellegrino, in *SPIE Newsroom*. (SPIE Newsroom, 2014).

[6] M. E. Farrell, E. L. Holthoff, P. M. Pellegrino, "Next generation Surface Enhanced Raman Scattering (SERS) substrates for Hazard Detection," SPIE 8358, 835816 (2012).

[7] M. E. Farrell, E. L. Holthoff, P. M. Pellegrino, "Surface-Enhanced Raman Scattering Detection of Ammonium Nitrate Samples Fabricated Using Drop-on-Demand Inkjet Technology," Appl. Spec. 68, 287 (2014).

[8] M. E. Farrell, E. L. Holthoff, P. M. Pellegrino, "Surface-Enhanced Raman Scattering Detection of Ammonium Nitrate Samples Fabricated Using Drop-on-Demand Inkjet Technology," Applied Spectroscopy 68, 287 (2014).

[9] L. Tian, S. Tadepalli, M. Farrell, K.-K. Liu, N. Gandra, P. Pellegrino *et al.*, "Plasmonic Calligraphy: Multiplexed Charge-Selective Surface Enhanced Raman Scattering Substrate," Nanotechnology Accepted, (2014).

[10] L. Tian, S. Tadepalli, M. E. Farrell, K.-K. Liu, N. Gandra, P. M. Pellegrino *et al.*, "Multiplexed charge-selective surface enhanced Raman scattering based on plasmonic calligraphy," Journal of Materials Chemistry C accepted, (2014).

[11] E. D. Emmons, J. A. Guicheteau, A. W. Fountain, III, S. D. Christesen, "Comparison of Visible and Near-Infrared Raman Cross-Sections of Explosives in Solution and in the Solid State," Appl Spectros 66, 636 (2012).

[12] C. K. Chan, M. N. Chan, "New Directions: Polymorphic transformation of ammonium nitrate in atmospheric aerosols," Atmos. Eviron. 38, 1387 (2004).

[13] C. S. Choi, J. E. Mapes, E. Prince, "Structure of ammonium nitrate (IV)," Acta Crystal. Sect. B-Struct. Cryst. Cryst.Chem. 28, 1357 (1972).

[14] R. J. Davey, P. D. Guy, A. J. Ruddick, "The IV- III polymophic phase transition in aqueous slurries of ammonium nitrate " J. Col. Interf. Sci. 108, 189 (1985).

[15] R. J. Davey, A. J. Ruddick, P. D. Guy, B. Mitchell, S. J. Maginn, L. A. Polywka, "The IV-III polymorphic phase-transition in ammonium nitrate - a unique example of solvent mediation," J. Phys. D. Apply. Phys 24, 176 (1991).
[16] R. M. Harrison, W. T. Sturgis, A.-M. N. Kitto, Y. Li, "Kinetics of Evaporation of Ammonium chloride and ammonium Nitrate Aerosols," Atmos. Environ. 24, 1883 (1990).
[17] J. R. Holden, C. W. Dickinson, "Crystal Structure of 2 solid solution phases of ammonium nitrate and pottasium nitrate," J. Phys. Chem. 79, 249 (1975).
[18] C. B. Richardson, R. L. Hightower, "Evaporation of ammonium nitrate particles," Atmos. Envir. 21, 971 (1987).
[19] E. D. Emmons, M. E. Farrell, E. L. Holthoff, A. Tripanthi, N. Green, R. P. Moon *et al.*, "Characterization of Polymorphic States in Energetic Samples of 1,3,5-Trinitro-1,3,5-Triazine (RDX) Fabricated Using Drop-on- Demand Inkjet Technology," Appl. Spectrosc. 66, 628 (2012).
[20] E. D. Emmons, M. E. Farrell, E. L. Holthoff, A. Tripathi, N. Green, R. P. Moon *et al.*, "Characterization of Polymorphic States in Energetic Samples of 1,3,5-Trinitro-1,3,5-Triazine (RDX) Fabricated Using Drop-on-Demand Inkjet Technology," Applied Spectroscopy 66, 628 (2012).
[21] M. Ghosh, L. Wang, S. A. Asher, "Deep-Ultraviolet Resonance Raman Excitation Profiles of NH4NO3, PETN, TNT, HMX, and RDX," Applied Spectroscopy 66, 1013 (2012).
[22] P. Torres, L. Mercado, I. Cotte, S. P. Hernadez, N. Mina, A. Santana *et al.*, "Vibrational Spectroscopy Study of B and A RDX Deposits," J. Phys. Chem. B 108, 8799 (2004).
[23] P. Torres, L. Mercado, L. Mortimer, N. Mina, S. Hernandez, R. Larau *et al.*, "Raman and scanning electron microscopy measurements of RDX on glass substrates," SPIE 5089, 1054 (2003).
[24] D. Bedrov, C. Ayyagari, G. D. Smith, T. D. Sewell, R. Menikoff, J. M. Zaug, "Molecular dynamics simulations of HMX crystal polymorphs using a flexible molecule force field," Journal of Computer-Aided Materials Design 8, 77 (2001).
[25] W. Zhu, J. Xiao, G. Ji, F. Zhao, H. Xiao, "First-principles study of the four polymorphs of crystalline octahydro-1,3,5,7-tetranitro-1,3,5,7-tetrazocine," Journal of Physical Chemistry B 111, 12715 (2007).
[26] T. M. Anish K. Goyal, Melissa Spencer, Matthew Aernecke, Rod R. Kunz, Stella Park, Bryan E. Tipton, Michael W. Kelly, Ellen L. Holthoff, Mikella E. Farrell, Paul M. Pellegrino,, "Active infrared hyperspectral imaging of solid particles on surfaces," SPIE 8710, (2013).
[27] E. L. Holthoff, M. E. Farrell, P. M. Pellegrino "Investigating a drop-on-demand microdispenser for standardized sample preparation," SPIE 8358:, 83580V (2012).
[28] E. L. Holthoff, M. E. Hankus, P. M. Pellegrino, "Investigating a drop-on-demand microdispenser for standardized sample preparation," SPIE 8018:, F1 (2011).
[29] M. E. Hankus, D. N. Stratis-Cullum, P. M. Pellegrino, "Characterization of next-generation commercial surface-enhanced Raman scattering (SERS) substrates," SPIE 8018:, P1 (2011).
[30] T. V. Brook, in *USA TODAY*. (2013).